

## Observation of Collapse and Revival in a Superconducting Atomic Frequency Comb

E. S. Redchenko<sup>1,2,\*</sup>, M. Zens<sup>3</sup>, M. Žemlička<sup>1</sup>, M. Peruzzo<sup>1</sup>, F. Hassani<sup>1</sup>, R. Sett<sup>1</sup>, P. Zieliński<sup>1</sup>, H. S. Dhar<sup>4,5</sup>,  
D. O. Krimer<sup>3</sup>, S. Rotter<sup>3</sup>, and J. M. Fink<sup>1,†</sup>

<sup>1</sup>*Institute of Science and Technology Austria, Am Campus 1, 3400 Klosterneuburg, Austria*


<sup>2</sup>*Vienna Center for Quantum Science and Technology, Atominstytut, TU Wien, Stadionallee 2, 1020 Vienna, Austria*

<sup>3</sup>*Institute for Theoretical Physics, TU Wien, Wiedner Hauptstraße 8-10/136, 1040 Vienna, Austria*

<sup>4</sup>*Department of Physics, Indian Institute of Technology Bombay, Powai, Mumbai 400076, India*

<sup>5</sup>*Centre of Excellence in Quantum Information, Computation, Science and Technology,*

*Indian Institute of Technology Bombay, Mumbai 400076, India*

 (Received 18 September 2023; revised 8 May 2024; accepted 2 January 2025; published 11 February 2025)

Recent advancements in superconducting circuits have enabled the experimental study of collective behavior of precisely controlled intermediate-scale ensembles of qubits. In this work, we demonstrate an atomic frequency comb formed by individual artificial atoms strongly coupled to a single resonator mode. We observe periodic microwave pulses that originate from a single coherent excitation dynamically interacting with the multiqubit ensemble. We show that this revival dynamics emerges as a consequence of the constructive and periodic rephasing of the five superconducting qubits forming the vacuum Rabi split comb. In the future, similar devices could be used as a memory with *in situ* tunable storage time or as an on-chip periodic pulse generator with nonclassical photon statistics.

DOI: [10.1103/PhysRevLett.134.063601](https://doi.org/10.1103/PhysRevLett.134.063601)

Collapse and revival of quantum excitations appear in many systems under different conditions [1–7] and have important imaging and memory applications [8,9]. One can modify the spontaneous exponential decay of an excited system into revival dynamics using spatial and temporal interference between atoms [1] or by coupling a system to a non-Markovian bath [2]. For a two-level atom interacting with a single mode of a cavity, quantum revivals were theoretically predicted [3,10] and experimentally observed [4,5] within the Jaynes-Cummings model [11]. Other examples of the collapse and revival dynamics include well-known spin and photon echos [6,7]. The conventional magnetic resonance Hahn echo sequence can lead to the train of periodic, self-stimulated revivals in a strong coupling regime [12,13], while modified photon echoes using atomic frequency combs (AFCs) can be used for storing photonic quantum states in atomic ensembles [9].

The revival in the AFC case corresponds to the collective retrieval of light after storage in a solid [14] and proves AFCs to be a promising memory platform primarily due to their high multimode capacity [15], long storage

times [16,17], and the capability of storing quantum states [18,19]. The storage efficiency, however, has to be further enhanced for quantum repeater applications [20], for instance, by coupling to a cavity [21]. Yet, most realizations use impedance-matched cavities since frequency combs get distorted by the cavity in the strong coupling limit [22].

A recent theoretical proposal showed how one can get around this limitation by spectral tuning the individual atoms and adjusting their coupling values [23]. There has been immense progress in addressing individual atoms within an atomic array [24], but the necessary degree of control of individual atom parameters is currently only offered by superconducting microwave circuits. Superconducting qubits have shown great potential for simulating many-body quantum systems [25–28]. The flexibility of the circuit design supports synthesizing various few [29,30] and many-body interaction Hamiltonians [31–33]. This ability to tune the coupling strength is vital for the generation of multiqubit entanglement in a quantum network [34]. Moreover, the rapid development of superconducting circuits over the last several decades has now allowed precise control over intermediate-sized systems [35–38].

In this Letter, we present the first superconducting AFC (sAFC) based on individual artificial atoms. Within this versatile system, superconducting transmon qubits can be individually tuned with high precision changing the inhomogeneity of the sAFC to produce cavity state revivals at well-defined and tunable times. The sAFC is realized on-chip with five transmon qubits capacitively coupled to the

\*Contact author: [elena.redchenko@tuwien.ac.at](mailto:elena.redchenko@tuwien.ac.at)

†Contact author: [johannes.fink@ist.ac.at](mailto:johannes.fink@ist.ac.at)

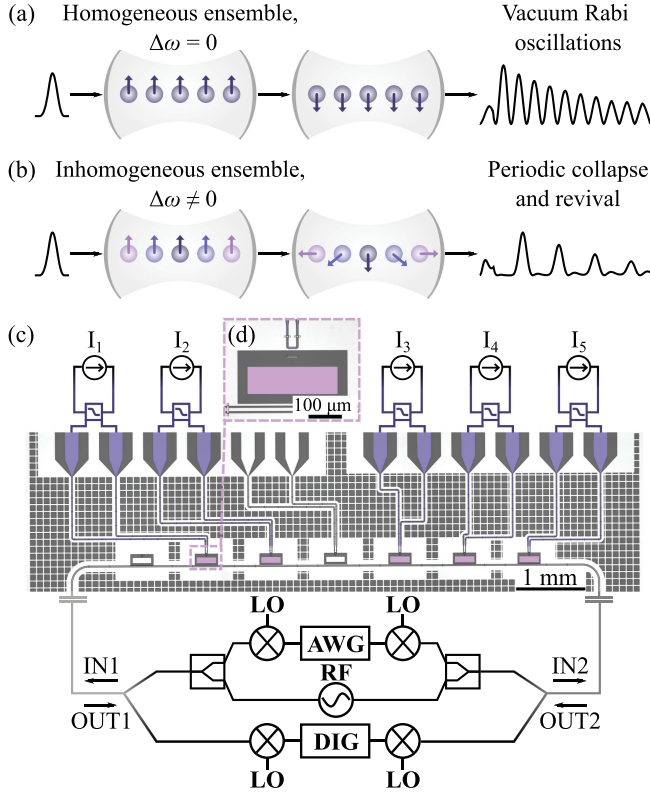


FIG. 1. (a) Schematic showing collective vacuum Rabi oscillations caused by a short excitation pulse in a resonant and homogeneous qubit ensemble,  $\Delta\omega = 0$ . (b) Schematic showing periodic pulse revivals caused by a short excitation pulse in an inhomogeneous qubit ensemble,  $\Delta\omega \neq 0$ . (c) Optical microscope image and simplified experimental setup. Seven transmon qubits are capacitively coupled to a coplanar waveguide resonator, and six qubits have a symmetric local flux bias line highlighted in purple. Qubits used in a sAFC are highlighted in pink. Each comb qubit is connected to a current source. The system gets continuous input from an RF source and pulsed input from the upconverted arbitrary waveform generator (AWG) signal. Analog down-conversion and digitization (DIG) are used to back out the scattering parameters of the device cooled to 10 mK. (d) Enlarged view of qubit and local symmetric flux bias line inductively coupled to the qubit SQUID.

microwave resonator. The central qubit is set in resonance with the cavity  $\omega = \omega_c$  while others are  $\pm\Delta\omega$  and  $\pm 2\Delta\omega$  detuned. In contrast to a resonant ensemble, shown in Fig. 1(a), where the collective vacuum Rabi oscillations are observed [39,40], in such an inhomogeneous ensemble [Fig. 1(b)], collectively excited qubits arranged in a sAFC rotate over the Bloch sphere at different speeds. The subensembles of qubits constructively rephase at regular intervals, which leads to a periodic photon emission corresponding to the collective transfer of excitations from the qubit ensemble to the resonator [41].

The studied system is described by the driven Tavis-Cummings Hamiltonian [42]:

$$\hat{H}_{\text{sys}} = \hat{H}_{\text{TC}} + \hat{H}_{\text{drive}}, \quad (1)$$

where

$$\begin{aligned} \hat{H}_{\text{TC}} = & \hbar\omega_c \hat{a}^\dagger \hat{a} + \frac{\hbar}{2} \sum_{k=1}^N \omega_k \hat{\sigma}_k^z \\ & + \hbar \sum_{k=1}^N g_k (\hat{\sigma}_k^- \hat{a}^\dagger + \hat{\sigma}_k^+ \hat{a}), \end{aligned} \quad (2)$$

$$\hat{H}_{\text{drive}} = i\hbar[\epsilon(t)\hat{a}^\dagger e^{-i\omega_d t} + \epsilon^*(t)\hat{a} e^{i\omega_d t}]. \quad (3)$$

Here  $g_k$  are the qubits' coupling strengths to the resonator,  $\omega_k$  are the qubits' frequencies,  $\omega_d$  is the excitation pulse frequency, and  $\epsilon(t) = \epsilon \text{erect}[(t - t_0)/2]/t_0$ , where  $\epsilon$  is the drive amplitude and  $t_0$  is the pulse duration.

We fabricate the sample with seven transmon qubits capacitively coupled to the first harmonic of a half-wavelength coplanar waveguide resonator (CPW) shown in Fig. 1(c). For the distance between qubits of  $600 \mu\text{m}$ , the simulated direct capacitive coupling between them  $g_{\text{cap}}/(2\pi) \approx 36 \text{ kHz}$  is negligible. We also do not observe any direct inductive coupling between qubits. Qubits used to form a sAFC are highlighted in pink. Six transmons have individual on-chip symmetric dc-bias lines inductively coupled to the SQUIDs as demonstrated in Fig. 1(d).

The first harmonic of the CPW has a resonance at  $\omega_c/(2\pi) = 5.878 \text{ GHz}$ . The internal loss of the resonator  $\kappa_i/(2\pi) \approx 3 \text{ kHz}$  is negligible compared to the full resonator bandwidth  $\kappa_{\text{load}}/(2\pi) \approx 0.93 \text{ MHz}$ . The average qubit coupling strength to the resonator is  $g/(2\pi) \sim 30 \text{ MHz}$ , and the on-resonance qubit decoherence parameters  $\gamma_k/(2\pi) < 600 \text{ kHz}$  were extracted from vacuum Rabi splitting measurements. See full sample characterization in Supplemental Material [43].

Symmetric dc-bias lines used in this device allow tuning the qubit frequency up to two flux quanta without introducing a significant flux crosstalk between qubits. An additional global flux offset can be created using the bias coil mounted on top of the sample box. The full flux quanta matrix and the calibration procedure can be found in Supplemental Material [43]. We demonstrate full frequency control by measuring the transmission amplitude as a function of measurement comb spacing  $\Delta\omega/(2\pi)$  and frequency and time, as shown in Figs. 2(a) and 2(b) respectively.

In the frequency domain, we measure the transmission spectrum of a qubit ensemble versus probe frequency  $\omega$  and comb spacing  $\Delta\omega$ , as shown in Fig. 2(a) where white dashed lines show the numerically calculated eigenvalues  $E_i$  ( $i = 1, \dots, 6$ ) of the Tavis-Cummings Hamiltonian [Eq. (2)]. For high comb spacings  $|\Delta\omega/(2\pi)| > 2g/(2\pi)$ , transmission is dominated by the vacuum Rabi splitting peaks of the central qubit, shown in Fig. 2(c). Approaching  $\Delta\omega/(2\pi) = 0$ , these dressed states then merge into two peaks that correspond to collective vacuum Rabi splitting

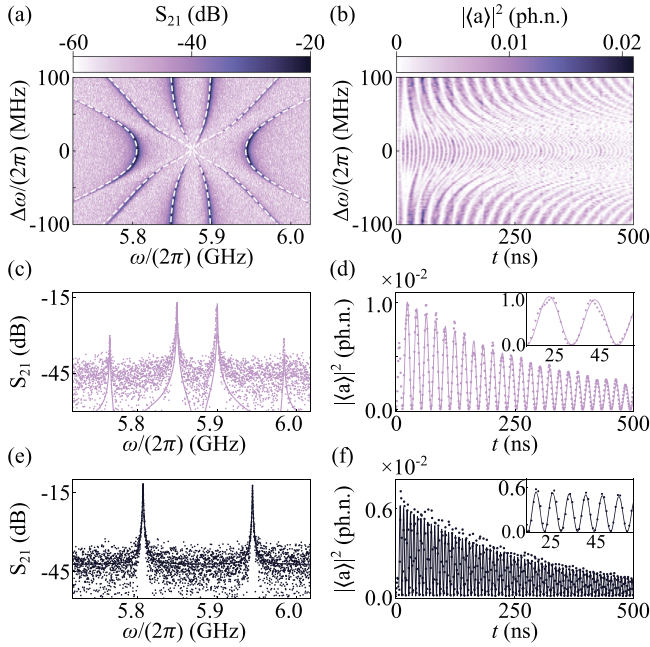


FIG. 2. (a) Measured resonator transmission spectrum of a five qubit ensemble as a function of probe frequency  $\omega$  and comb spacing  $\Delta\omega$ . White dashed lines are the calculated eigenvalues. (b) Squared absolute value of the transmission amplitude  $|\langle a \rangle|^2$  measured as a function of time  $t$  and comb spacing  $\Delta\omega$ . (c),(e) Transmission spectrum of a five qubit ensemble as a function of probe frequency  $\omega$  for comb spacing  $\Delta\omega/(2\pi)$  of 100 MHz and 0 MHz, respectively. (d),(f) Single qubit [ $\Delta\omega/(2\pi) = 100$  MHz] and collective ( $\Delta\omega/(2\pi) = 0$  MHz) vacuum Rabi oscillations.

with the collective coupling frequency  $G/(2\pi) = \sqrt{\sum_{i=k}^5 g_k^2} = 68.95$  MHz, shown in Fig. 2(e).

In the time domain measurements, shown in Fig. 2(b), the system is excited by the short (6 ns) pulse which is generated using up-conversion of the output signal from the arbitrary waveform generator. The pulse amplitude  $\epsilon \sim 5\kappa_{\text{load}}$  in this measurement corresponds to the input power of 25 photons in the case of the empty cavity with  $\kappa_{\text{load}}$  bandwidth. Transmission amplitude is then recorded by the digitizer in volts at high (250 MHz) intermediate frequency matching the instantaneous bandwidth of the detection chain. For high comb spacings  $|\Delta\omega/(2\pi)| > 2g/(2\pi)$ , we observe vacuum Rabi oscillations of the central qubit with frequency  $\omega_{\text{Rabi}}/(2\pi) = 49.6$  MHz  $\approx 2g/(2\pi)$ , as shown in Fig. 2(d) where the solid line is the data fit with damped sinusoidal function,  $f(t) = e^{-\Gamma t}(\sin \Omega t + 1)$ . For close to zero detunings, we see the expected collective vacuum Rabi oscillations, shown in Fig. 2(f). Now, the oscillation frequency extracted from the damped sinusoidal fit  $\omega_{\text{colRabi}}/(2\pi) = 137.4$  MHz is close to the collective vacuum Rabi splitting  $2G/(2\pi) = 137.9$  MHz. Moreover, in both cases of single and collective vacuum Rabi oscillations, we find that decay parameter

$\Gamma/(2\pi) \approx 0.5$  MHz  $\sim (\kappa_{\text{load}} + \overline{\gamma_k})/(4\pi)$ , where  $\overline{\gamma_k}$  is an average of qubit decoherence parameters.

For the intermediate comb spacings  $g \lesssim \Delta\omega \lesssim 2g$ , we observe six bright dressed states  $E_i$  of the five-qubit ensemble coupled to the resonator in the frequency domain, see Fig. 2(a). In the time domain, when the short pulse is sent to the sAFC, the system exhibits a pulsed collapse and revival dynamics. In Fig. 3(a), black dots demonstrate the extracted revival time  $\tau$  from Fig. 2(b) defined as the hold time between the transmitted pulse and the first revival as a function of the frequency difference between the respective neighboring bright states  $\Delta E_i$  ( $i = 1, \dots, 5$ ) obtained from Fig. 2(a). The revival time decay with the increase of the comb spacing and the dashed line shows the expected  $\tau = 2\pi/\Delta E_i$  trend [23,41]. The error bars indicate the standard deviation from the mean value of  $\Delta E_i$ . High error values (up to  $\sim 6$  MHz for small combs) come from the spectral distortion of the sAFC due to strong coupling to the resonator [23] while the positioning of qubits in the comb is implemented with up to  $\sim 1$  MHz precision.

Colored dots in Fig. 3(a) indicate the storage time for the comb spacing of  $\Delta\omega/(2\pi) = 35, 40, 45,$  and 50 MHz measured separately at  $\epsilon \sim 2.5\kappa_{\text{load}}$  drive amplitude. We first measure the system in the frequency domain to identify the qubits' spectral positions precisely. The transmission spectra, shown in Fig. 3(b), are fitted using the function derived from the steady-state Maxwell-Bloch equations:

$$S(\omega) = \frac{A}{\kappa_{\text{load}}/2 + i(\omega_c - \omega) + \sum_{k=1}^5 \frac{g_k^2}{\gamma_k^2 + i(\omega_k - \omega)}}. \quad (4)$$

The fit relies on the qubits' parameters extracted from the vacuum Rabi splitting measurements ( $g_k$  and  $\gamma_k$ ). The qubits' spectral positions  $\omega_k$  and the dimensionless amplitude  $A$  given by attenuation and amplification in the setup are kept as free parameters.

The time evolution of the system can be theoretically predicted by solving the Lindblad master equation [41]:

$$\rho = -\frac{i}{\hbar} [\hat{H}_{\text{sys}}, \rho] + \kappa_{\text{load}} \mathcal{L}_{\hat{a}}[\rho] + \sum_k \gamma_k \mathcal{L}_{\sigma_k}[\rho], \quad (5)$$

where  $\mathcal{L}_{\hat{a}} = \hat{a}$  is the Lindblad operator corresponding to the resonator losses and the qubit decay is accounted for by  $\mathcal{L}_{\sigma_k} = \sigma_k^-$ .

We numerically solve Eq. (5) in PYTHON using QuTip [48] for the extracted qubit positions and find the behavior of the coherent cavity response  $|\langle a \rangle|^2$ . Time traces shown in Fig. 3(c) were scaled to the numerically predicted value. We see excellent agreement between the theoretically predicted and experimentally observed microwave revival dynamics. The revival time for these comb spacings was extracted from the first six peaks excluding one overlapping with the beat mode on top of the revivals. The error of

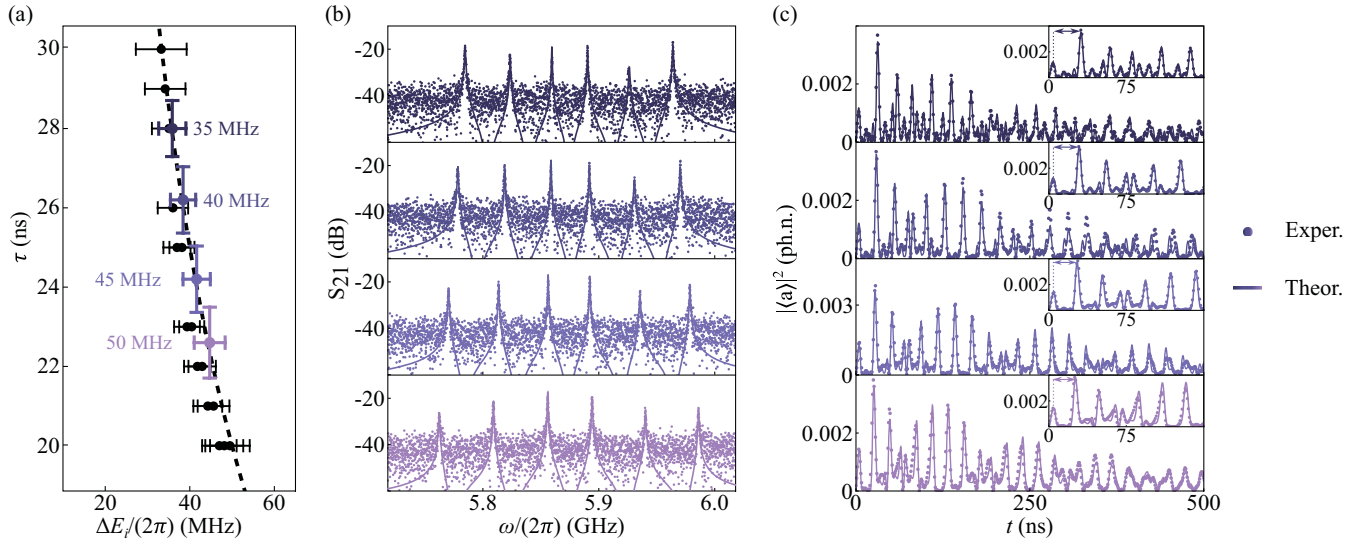


FIG. 3. (a) The revival time  $\tau$  as a function of the mean frequency difference between the respective neighboring bright states  $\Delta E_i$  ( $i = 1, \dots, 5$ ) extracted from Fig. 2(b). (b) Transmission spectra of a five qubit ensemble measured as a function of probe frequency  $\omega$  for comb spacing  $\Delta\omega/(2\pi) = 35, 40, 45, 50$  MHz. Solid lines are fitted with Eq. (4). (c) Squared absolute value of the transmission amplitude measured as a function of time  $t$  for same detuning frequencies as shown in (b). Solid lines are numerical solutions of Eq. (5). Insets demonstrate transmitted excitation pulse and approximately five first revivals, where the first storage time is indicated with an arrow.

0.8 ns is below the  $\sim 2$  ns time resolution in our system. The beating on top of the revival dynamics arises from the nonequidistant spacing of the bright states  $\Delta E_i$ , which is partially caused by the slight differences in the coupling strength  $g_k$ . The additional noise between revivals in Fig. 3(c) comes from the finite ensemble size where the system is found in a mix between vacuum Rabi oscillations and full constructive or destructive rephasings. The decay of the revival dynamics is dominated by the resonator coupling  $\kappa_{\text{load}}$ .

Our system based on an sAFC can operate in a wide range of input powers, which is explained by two characteristic features. First of all, as we deal with a multiqubit system, which has a higher cumulative absorption, it can handle higher input photon numbers before getting saturated (approximately five photons, in our case). Measurements on the power dependence of the sAFC and of a single resonant qubit in a cavity reveal that the dressed states of the qubit ensemble get saturated at least at  $\sim 6$  dB higher probe power than the dressed states of a single qubit, which is indicated with black dashed lines in Figs. 4(a) and 4(b). Second, the sAFC acts as a filter for the excitation pulse. According to our estimations based on the integrated overlap of the comb and pulse envelopes in the frequency domain, only  $\sim 1/25$  of the excitation pulse power is absorbed by the qubit ensemble, see Supplemental Material [43]. Hence, sending excitation pulses with an amplitude scaling from  $\epsilon \approx 0.3\kappa_{\text{load}}$  to  $\epsilon \approx 6.2\kappa_{\text{load}}$ , corresponding to 0.1 to a 38 input photon power, does not break revivals. We observe the distortion of the pulse revivals at

drive amplitude around  $\epsilon \approx 26.3\kappa_{\text{load}}$  or 695 photons, while the clear destruction of revival dynamics happens at  $\epsilon \approx 42\kappa_{\text{load}}$  or 1764 photons. The theoretically predicted coherent cavity response is shown with the solid line in Fig. 4(c).

Overall, signatures of the constructive rephasing in the qubit ensemble are observable in a  $\sim 30$  dB range of input powers. The operating power range can be further expanded with an increase in the number of qubits in the ensemble, which also makes the pulses sharper [41]. This property allows one to use sAFCs as temporal power dividers or periodic signal generators—as a strong coherent input pulse is split by the sAFC into temporally equidistant single photon revivals. In this operation regime, our device has a potential as a high-rate nonclassical photon source [49].

In conclusion, we have studied the collapse and revival dynamics of a microwave pulse in an inhomogeneous superconducting qubit ensemble that forms the first sAFC made of individual emitters. Because of its high reconfigurability it can act as a test bed for classical AFC operation. The revival time of the observed tunable periodic pulses is controlled *in situ* by variation of the comb spacing  $\Delta\omega$  through a change in the bias settings. For small comb spacings, our system with its increased storage time operates as a coherent microwave memory. AFC-inspired memory devices are particularly useful for the storage of arbitrary multiphoton states. Remarkably, in contrast to the realization with multiresonators [50,51], the sAFC approach benefits from the efficient information transfer

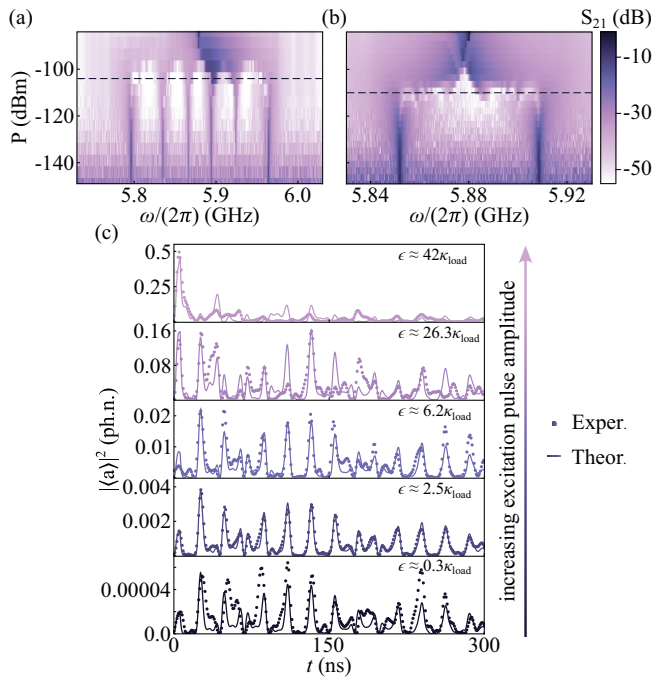


FIG. 4. Transmission spectra of a five qubit ensemble with a comb spacing  $\Delta\omega/(2\pi) = 30$  MHz (a) and a single qubit vacuum Rabi splitting (b) measured as a function of probe frequency  $\omega$  and probe power  $P$ . (c) Squared absolute value of the transmission amplitude measured as a function of time  $t$  for different drive amplitudes  $\epsilon$  for comb spacing  $\Delta\omega/(2\pi) = 50$  MHz.

enabled by the strong coupling regime, which leads to potential storage fidelities near unity also for non-Gaussian cavity states, which is important for quantum memory protocols [23]. When the comb spacing is large, the high repetition rate of the revivals together with the enhanced power handling enables this on-chip integrated device to be used as a periodic signal generator that outputs time-constrained pulses at regular intervals. Based on their quantum nature, sAFCs have a prospect to act as periodic nonclassical microwave sources for timing in quantum networks [52]. Combining the demonstrated sAFC with fast time-domain control of the qubit frequencies, excitations, and tomography, one can utilize these fast interactions within sAFC for the preparation and distribution of quantum states in qubit ensembles rather than individual atoms [53,54]. The achieved high degree of control over multiqubit ensembles not only opens the door to exploring a new regime of light-matter interaction and quantum simulations of many-body dynamics but also represents another step toward new applications in future superconducting quantum computing hardware.

*Acknowledgments*—The authors thank G. Arnold and R. Sahu for the discussions, L. Drmic for software development, the MIBA workshop and the ISTA nanofabrication facility for technical support, and VTT Technical Research Centre of Finland for providing us TWPAs for follow-up

measurements. This work was supported by the Austrian Science Fund (FWF) [Grant DOI: 10.55776/F71] through BeyondC (F7105) and IST Austria. E. S. R. is the recipient of a DOC fellowship of the Austrian Academy of Sciences at IST Austria. J. M. F. and M. Ž. acknowledge support from the European Research Council under Grant Agreement No. 758053 (ERC StG QUNNECT) and a NOMIS foundation research grant.

*Data availability*—All data used in this study are available in Ref. [55].

- [1] S. Mährlein, L. Götzendörfer, K. Günthner, J. Evers, and J. von Zanthier, Birth, death, and revival of spontaneous emission in a three-atom system, *Phys. Rev. Res.* **2**, 013278 (2020).
- [2] V. S. Ferreira, J. Banker, A. Sipahigil, M. H. Matheny, A. J. Keller, E. Kim, M. Mirhosseini, and O. Painter, Collapse and revival of an artificial atom coupled to a structured photonic reservoir, *Phys. Rev. X* **11**, 041043 (2021).
- [3] J. H. Eberly, N. B. Narozhny, and J. J. Sanchez-Mondragon, Periodic spontaneous collapse and revival in a simple quantum model, *Phys. Rev. Lett.* **44**, 1323 (1980).
- [4] G. Rempe, H. Walther, and N. Klein, Observation of quantum collapse and revival in a one-atom maser, *Phys. Rev. Lett.* **58**, 353 (1987).
- [5] M. Brune, F. Schmidt-Kaler, A. Maali, J. Dreyer, E. Hagley, J. Raimond, and S. Haroche, Quantum Rabi oscillation: A direct test of field quantization in a cavity, *Phys. Rev. Lett.* **76**, 1800 (1996).
- [6] E. L. Hahn, Spin echoes, *Phys. Rev.* **80**, 580 (1950).
- [7] I. D. Abella, N. A. Kurnit, and S. R. Hartmann, Photon echoes, *Phys. Rev.* **141**, 391 (1966).
- [8] B. A. Jung and M. Weigel, Spin echo magnetic resonance imaging, *J. Magn. Reson. Imaging* **37**, 805 (2013).
- [9] M. Afzelius, C. Simon, H. de Riedmatten, and N. Gisin, Multimode quantum memory based on atomic frequency combs, *Phys. Rev. A* **79**, 052329 (2009).
- [10] D. Lechner, R. Pennetta, M. Blaha, P. Schneeweiss, A. Rauschenbeutel, and J. Volz, Light-matter interaction at the transition between cavity and waveguide QED, *Phys. Rev. Lett.* **131**, 103603 (2023).
- [11] E. Jaynes and F. Cummings, Comparison of quantum and semiclassical radiation theories with application to the beam maser, *Proc. IEEE* **51**, 89 (1963).
- [12] K. Debnath, G. Dold, J. J. L. Morton, and K. Mølmer, Self-stimulated pulse echo trains from inhomogeneously broadened spin ensembles, *Phys. Rev. Lett.* **125**, 137702 (2020).
- [13] S. Weichselbaumer, M. Zens, C. W. Zollitsch, M. S. Brandt, S. Rotter, R. Gross, and H. Huebl, Echo trains in pulsed electron spin resonance of a strongly coupled spin ensemble, *Phys. Rev. Lett.* **125**, 137701 (2020).
- [14] H. De Riedmatten, M. Afzelius, M. U. Staudt, C. Simon, and N. Gisin, A solid-state light-matter interface at the single-photon level, *Nature (London)* **456**, 773 (2008).
- [15] A. Ortu, J. V. Rakonjac, A. Holzäpfel, A. Seri, S. Grandi, M. Mazzer, H. de Riedmatten, and M. Afzelius, Multimode

- capacity of atomic-frequency comb quantum memories, *Quantum Sci. Technol.* **7**, 035024 (2022).
- [16] C. Laplane, P. Jobez, J. Etesse, N. Timoney, N. Gisin, and M. Afzelius, Multiplexed on-demand storage of polarization qubits in a crystal, *New J. Phys.* **18**, 013006 (2015).
- [17] A. Holzäpfel, J. Etesse, K. T. Kaczmarek, A. Tiranov, N. Gisin, and M. Afzelius, Optical storage for 0.53 s in a solid-state atomic frequency comb memory using dynamical decoupling, *New J. Phys.* **22**, 063009 (2020).
- [18] E. Saglamyurek, N. Sinclair, J. Jin, J. A. Slater, D. Oblak, F. Bussières, M. George, R. Ricken, W. Sohler, and W. Tittel, Broadband waveguide quantum memory for entangled photons, *Nature (London)* **469**, 512 (2011).
- [19] C. Laplane, P. Jobez, J. Etesse, N. Gisin, and M. Afzelius, Multimode and long-lived quantum correlations between photons and spins in a crystal, *Phys. Rev. Lett.* **118**, 210501 (2017).
- [20] H.-J. Briegel, W. Dür, J. I. Cirac, and P. Zoller, Quantum repeaters: The role of imperfect local operations in quantum communication, *Phys. Rev. Lett.* **81**, 5932 (1998).
- [21] P. Jobez, I. Usmani, N. Timoney, C. Laplane, N. Gisin, and M. Afzelius, Cavity-enhanced storage in an optical spin-wave memory, *New J. Phys.* **16**, 083005 (2014).
- [22] M. Afzelius and C. Simon, Impedance-matched cavity quantum memory, *Phys. Rev. A* **82**, 022310 (2010).
- [23] M. Zens, D. O. Krimer, H. S. Dhar, and S. Rotter, Periodic cavity state revivals from atomic frequency combs, *Phys. Rev. Lett.* **127**, 180402 (2021).
- [24] Z. Yan, J. Ho, Y.-H. Lu, S. J. Masson, A. Asenjo-Garcia, and D. M. Stamper-Kurn, Superradiant and subradiant cavity scattering by atom arrays, *Phys. Rev. Lett.* **131**, 253603 (2023).
- [25] A. F. van Loo, A. Fedorov, K. Lalumière, B. C. Sanders, A. Blais, and A. Wallraff, Photon-mediated interactions between distant artificial atoms, *Science* **342**, 1494 (2013).
- [26] M. Dalmonte, S. I. Mirzaei, P. R. Muppalla, D. Marcos, P. Zoller, and G. Kirchmair, Realizing dipolar spin models with arrays of superconducting qubits, *Phys. Rev. B* **92**, 174507 (2015).
- [27] N. Lambert, Y. Matsuzaki, K. Kakuyanagi, N. Ishida, S. Saito, and F. Nori, Superradiance with an ensemble of superconducting flux qubits, *Phys. Rev. B* **94**, 224510 (2016).
- [28] P. Song, Z. Xiang, Y.-X. Zhang, Z. Wang, X. Guo, X. Ruan, X. Song, K. Xu, Y. Y. Gao, H. Fan, and D. Zheng, Coherent control of Bloch oscillations in a superconducting circuit, *PRX Quantum* **5**, 020302 (2024).
- [29] J. Fink, M. Göppl, M. Baur, R. Bianchetti, P. Leek, A. Blais, and A. Wallraff, Climbing the Jaynes–Cummings ladder and observing its nonlinearity in a cavity QED system, *Nature (London)* **454**, 315 (2008).
- [30] O. Astafiev, A. M. Zagoskin, A. Abdumalikov, Y. A. Pashkin, T. Yamamoto, K. Inomata, Y. Nakamura, and J. S. Tsai, Resonance fluorescence of a single artificial atom, *Science* **327**, 840 (2010).
- [31] J. Puertas Martínez, S. Léger, N. Gheeraert, R. Dassonneville, L. Planat, F. Foroughi, Y. Krupko, O. Buisson, C. Naud, W. Hasch-Guichard *et al.*, A tunable Josephson platform to explore many-body quantum optics in circuit-QED, *npj Quantum Inf.* **5**, 19 (2019).
- [32] K. Zhang, H. Li, P. Zhang, J. Yuan, J. Chen, W. Ren, Z. Wang, C. Song, D.-W. Wang, H. Wang *et al.*, Synthesizing five-body interaction in a superconducting quantum circuit, *Phys. Rev. Lett.* **128**, 190502 (2022).
- [33] N. Mehta, R. Kuzmin, C. Ciuti, and V. E. Manucharyan, Down-conversion of a single photon as a probe of many-body localization, *Nature (London)* **613**, 650 (2023).
- [34] Y. Zhong, H.-S. Chang, A. Bienfait, É. Dumur, M.-H. Chou, C. R. Conner, J. Grebel, R. G. Povey, H. Yan, D. I. Schuster *et al.*, Deterministic multi-qubit entanglement in a quantum network, *Nature (London)* **590**, 571 (2021).
- [35] C. Song *et al.*, 10-qubit entanglement and parallel logic operations with a superconducting circuit, *Phys. Rev. Lett.* **119**, 180511 (2017).
- [36] Z. Wang, H. Li, W. Feng, X. Song, C. Song, W. Liu, Q. Guo, X. Zhang, H. Dong, D. Zheng *et al.*, Controllable switching between superradiant and subradiant states in a 10-qubit superconducting circuit, *Phys. Rev. Lett.* **124**, 013601 (2020).
- [37] P. Yang, J. D. Brehm, J. Leppäkangas, L. Guo, M. Marthaler, I. Boventer, A. Stehli, T. Wolz, A. V. Ustinov, and M. Weides, Probing the Tavis–Cummings level splitting with intermediate-scale superconducting circuits, *Phys. Rev. Appl.* **14**, 024025 (2020).
- [38] G. S. Mazhorin, I. N. Moskalenko, I. S. Besedin, D. S. Shapiro, S. V. Remizov, W. V. Pogosov, D. O. Moskalev, A. A. Pishchimova, A. A. Dobronosova, I. A. Rodionov, and A. V. Ustinov, Cavity-QED simulation of a quantum metamaterial with tunable disorder, *Phys. Rev. A* **105**, 033519 (2022).
- [39] Y. Kaluzny, P. Goy, M. Gross, J. M. Raimond, and S. Haroche, Observation of self-induced Rabi oscillations in two-level atoms excited inside a resonant cavity: The ringing regime of superradiance, *Phys. Rev. Lett.* **51**, 1175 (1983).
- [40] J. Fink, R. Bianchetti, M. Baur, M. Göppl, L. Steffen, S. Filipp, P. Leek, A. Blais, and A. Wallraff, Dressed collective qubit states and the Tavis–Cummings model in circuit QED, *Phys. Rev. Lett.* **103**, 083601 (2009).
- [41] H. S. Dhar, M. Zens, D. O. Krimer, and S. Rotter, Variational renormalization group for dissipative spin-cavity systems: Periodic pulses of nonclassical photons from mesoscopic spin ensembles, *Phys. Rev. Lett.* **121**, 133601 (2018).
- [42] M. Tavis and F. W. Cummings, Exact solution for an  $n$ -molecule—radiation-field Hamiltonian, *Phys. Rev.* **170**, 379 (1968).
- [43] See Supplemental Material at <http://link.aps.org/supplemental/10.1103/PhysRevLett.134.063601>, which includes Refs. [23,44–47], for details of (S1) Sample design; (S2) Sample characterization; (S3) Frequency comb preparation; (S4) Pulse power calibration.
- [44] P. Krantz, M. Kjaergaard, F. Yan, T. P. Orlando, S. Gustavsson, and W. D. Oliver, A quantum engineer’s guide to superconducting qubits, *Appl. Phys. Rev.* **6**, 021318 (2019).
- [45] F. Yan, P. Krantz, Y. Sung, M. Kjaergaard, D. L. Campbell, T. P. Orlando, S. Gustavsson, and W. D. Oliver, Tunable coupling scheme for implementing high-fidelity two-qubit gates, *Phys. Rev. Appl.* **10**, 054062 (2018).
- [46] A. Ryser and A. Wallraff, *Semester Thesis-Qubit Simulation and Design*, (ETH Zurich, Zurich, 2014).

- [47] E. M. Purcell, Spontaneous emission probabilities at radio frequencies, in *Confined Electrons and Photons* (Springer, New York, 1995), pp. 839–839, [10.1007/978-1-4615-1963-8\\_40](https://doi.org/10.1007/978-1-4615-1963-8_40).
- [48] J. Johansson, P. Nation, and F. Nori, Qutip: An open-source python framework for the dynamics of open quantum systems, *Comput. Phys. Commun.* **183**, 1760 (2012).
- [49] K. Wakui, Y. Tsujimoto, M. Fujiwara, I. Morohashi, T. Kishimoto, F. China, M. Yabuno, S. Miki, H. Terai, M. Sasaki *et al.*, Ultra-high-rate nonclassical light source with 50 GHz-repetition-rate mode-locked pump pulses and multiplexed single-photon detectors, *Opt. Express* **28**, 22399 (2020).
- [50] S. A. Moiseev, F. F. Gubaidullin, R. S. Kirillov, R. R. Latypov, N. S. Perminov, K. V. Petrovnin, and O. N. Sherstyukov, Multiresonator quantum memory, *Phys. Rev. A* **95**, 012338 (2017).
- [51] Z. Bao, Z. Wang, Y. Wu, Y. Li, C. Ma, Y. Song, H. Zhang, and L. Duan, On-demand storage and retrieval of microwave photons using a superconducting multiresonator quantum memory, *Phys. Rev. Lett.* **127**, 010503 (2021).
- [52] H. J. Kimble, The quantum internet, *Nature (London)* **453**, 1023 (2008).
- [53] V. S. Ferreira, G. Kim, A. Butler, H. Pichler, and O. Painter, Deterministic generation of multidimensional photonic cluster states with a single quantum emitter, *Nat. Phys.* **20**, 865 (2024).
- [54] B. Kannan, A. Almanakly, Y. Sung, A. Di Paolo, D. A. Rower, J. Braumüller, A. Melville, B. M. Niedzielski, A. Karamlou, K. Serniak *et al.*, On-demand directional microwave photon emission using waveguide quantum electrodynamics, *Nat. Phys.* **19**, 394 (2023).
- [55] E. Redchenko, M. Zens, M. Zemlicka, M. Peruzzo, F. Hassani, R. Sett, P. Zielinski, H. Dhar, D. Krimer, S. Rotter, and J. Fink, Observation of collapse and revival in a superconducting atomic frequency comb, [10.5281/zenodo.10808499](https://doi.org/10.5281/zenodo.10808499) (2024).